Memoirs of the Faculty of Science, Kyoto University, Series of Physics, Astrophysics, Geophysics and Chemistry, Vol. XXXIV, No. 2. Article 5, 1973.

NEUTRAL PION PHOTOPRODUCTION FROM HYDROGEN AT FORWARD ANGLES IN THE ENERGY RANGE 350 - 1175 MeV

BY

Akihiro MAKI

Department of Physics, Fuculty of Science, Kyoto University, Kyoto

(Received February 28, 1972)

ABSTRUCT

The differential cross sections near zero degree of the reaction $\gamma P \to \pi^\circ P$ in the energy range from 350 MeV to 1175 MeV were measured by detecting two photons from π° mesons. The angular dependences of the differential cross sections from zero degree to 50° in the CM system at about 600 MeV and 1000 MeV were also measured with the same method. The data were analysed with the similar method of Walker's partial wave analysis. This analysis required a rather large contribution of P_{11} wave in π° meson photoproduction from protons.

1. Introduction

Many experimental and theoretical efforts have been devoted in the field of single pion photoproductions in the resonance energy region for more than two decades. Some characteristics of large resonant waves, such as P_{33} and D_{13}, have been clarified, but many other important features have been left unclear because of the difficulties of photoproduction researches. On the other hand the knowledge on π N scattering has provided the useful informations on the nucleon resonances.

Recently there are increasing interests in the problem concerning to the similarity and difference between π N scattering and pion photoproduction. This problem becomes very important when the structure of hadrons is discussed. In the view point of quark model, pions are considered to be composed of a pair of a quark and an antiquark, but photons are considered to be elementary. The model predicts some selection rules for the photoproduction processes.[1)-4)] Indeed there seem to be some indications that the two processes have different features. Some resonant states which have been established in π N scattering have not been established in photoproduction. They are P_{11} (1470), S_{11} (1561), S_{11} (1715), S_{31} (1692) and so on.

These states have spins of 1/2 and can not be excited by the initrial-helicity-3/2 amplitude. On the other hand the large resonant states, P_{33} (1236), D_{13} (1518) and F_{15} (1688) can be excited by both helicity amplitudes. Among them, the D_{13} (1518) and F_{15} (1688) resonant states seem to be excited mainly by the initial-helicity-3/2 amplitudes.[4)-6)] According to the conservation of the angular momentum, only the initial-helicity-1/2 amplitudes are non-vanishing amplitudes at 0° or 180°. Therefore the differential cross sections of the reaction $\gamma p \to \pi^\circ p$ at 0° or 180° are more sensitive to study the small resonant states having spin 1/2 than those at other angles or total cross sections.

Ideally, to test the theoretical predictions, a comprete partial wave analysis of the data is desirable. There have been many theoretical and phenomenological partial wave analyses of pion photoproduction data.[7)-14)] Some of them can reproduce experimental data very well, but most of them were limitted in the energy region. Among these analyses there are some discrepancies. Overall understanding of pion photoproduction over the whole resonance region has not been obtained mainly due to the lack of comprete set of precise data, especially on the neutral pion production process. The precise and systematic measurements of the differential cross sections at 0° or 180° are important to evaluate the small amplitudes of the initial-helicity-1/2 without distervances by the large resonant waves of the initial-helicity-3/2.

We report here the results of the measurements of the differential cross sections of the reaction $\gamma p \rightarrow \pi^\circ p$ near zero degree in the energy range from 350 MeV to 1175 MeV and in the angular range from zero to 50 degrees in the CM system at about 600 MeV and 1000 MeV. We also analysed our data with the similar method of Walker's partial wave analysis.

2. Experimental Procedure

2-1 General Procedure

Fig. 1 shows a plan view of the experimental area. The bremsstrahlung beam from the 1.3 BeV electron synchrotron at the Institute for Nuclear Study, University of Tokyo, was incidented on a hydrogen target. The energies and correlation angle of two photons from the π° meson which was produced with the $\gamma p \rightarrow \pi^\circ p$ reaction were measured by a pair of photon detectors. In order to measure the energy dependence of the differential cross sections near zero degree, two photon detectors were set symmetrically at each side of the beam axis facing to the hydrogen target. The openning angle between the photon detectors was chosen to be equal to the minimum correlation angle of two photons from π° meson. Therefore the photon detectors were set at very small angles (i.e. 7.5°–22.5° depending on the energy of π°-mesons) with respect to the bremsstrahlung beam.

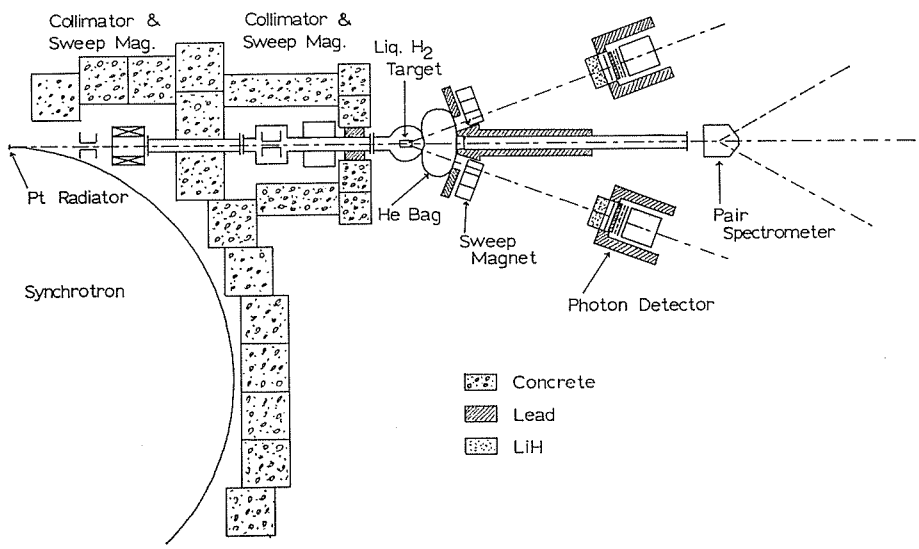

Fig. 1. Schematic diagram of the experimental arrangement for the zero degree measurements.

As is shown in Fig. 1, many devices were used to reduce heavy background due to the electromagnetic processes. These devices are:

(1) two pairs of collimators and sweep magnets to reduce a hallo of the incident beam,
(2) a helium bag and a vacuum duct were placed along the bremsstrahlung beam to remove air from the beam path,
(3) a pair of sweep magnets, which were placed between the hydrogen target and the photon detectors to sweep out charged particles, especially electrons and positrons, and have a rectangular aperture of 15 cm wide, 10 cm high and 20 cm long and a magnetic field of about 5 K Gauss.
(4) a pair of LiH hardeners of 0.2 radiation lengths in front of the photon detectors to reduce low energy photons, and
(5) many lead bricks for shielding.

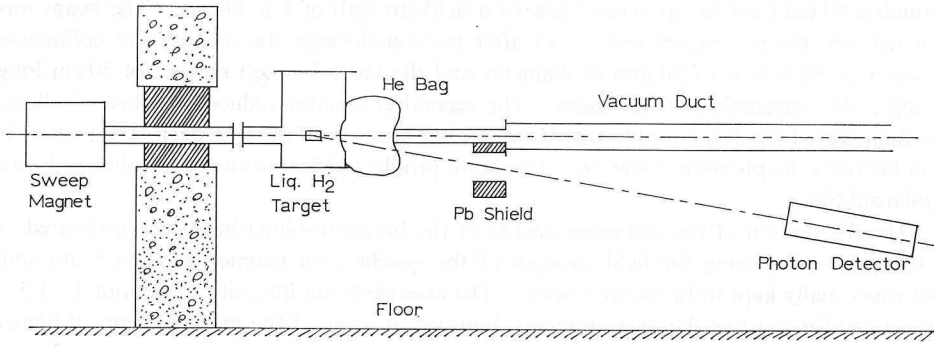

Fig. 2. Schematic diagram of the experimental arrangement for the small angles measurements (see text)

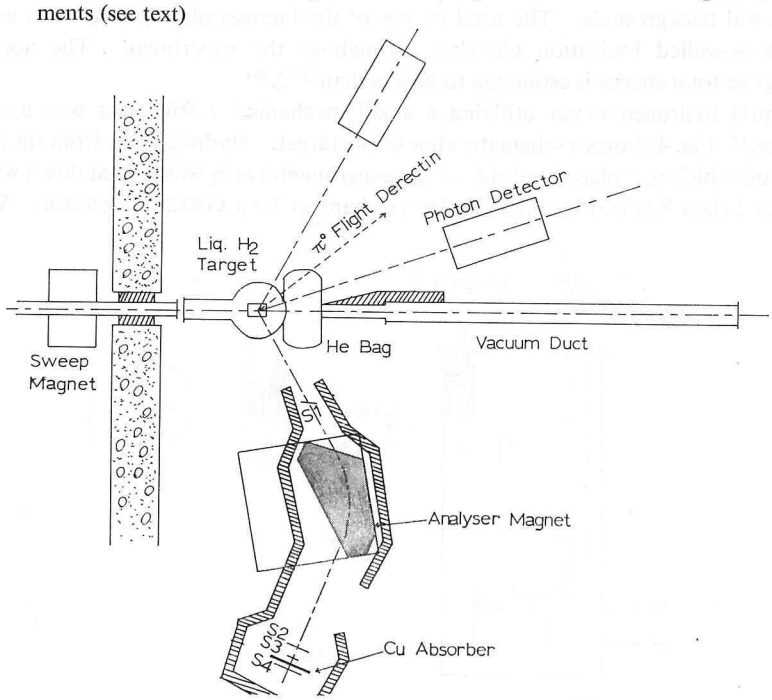

Fig. 3. Schematic diagram of the experimental arrangement for the large angles measurements and the calibration runs.

The angular dependence of the differential cross sections was also measured in the angular range from zero degree to 50 degrees in the CM system at the photon energies of about 600 MeV and 1000 MeV. As is shown in Fig. 2, both photon detectors were placed symmetrically with respect to the bremsstrahlung beam, however, the detectors were moved downward so that the π° mesons produced at the large angles could be measured with the photon detectors. A few measurements at large angles ($\theta_{\pi^\circ}{}^{Cm} \simeq 50^\circ$) have been performed by placing both photon detectors in the same side of the beam lines as is shown in Fig. 3.

2-2 Beam and target

Electrons accelerated in the synchrotron striked on a 50 μm thick platinum radiator and produced the bremsstrahlung beam. The beam was collimated by a lead collimator having a circular hole of 5 mm in diameter at 2.5 m from the radiator. Then it passed through a 50 cm long sweep magnet having a field strength of 7 K Gauss. The beam was then led into the γ–3 experimental area after passing through the second lead collimator having a circular hole of 20 mm in diameter and the second sweep magnet of 50 cm long having a field strength of 6 K Gauss. The second collimator reduced the beam halloes. The diameter of the beam profile was 22 mm at the position of the hydrogen target where is 10 m far from the platinum radiator. The beam profile and its position were observed with a polaroid film.

The fractuation of the end point energy of the bremsstrahlung beam was estimated to be 0.2% by monitoring the field strength of the synchrotron magnet.[15] The beam spill time was usually kept to be about 3 msec. The average beam intensity was about $1 \sim 1.5 \times 10^9$ e.q./sec for most of the measurements, however at some of the measurements at higher energies the beam intensity was reduced to about one-third of the average value to reduce the accidental backgrounds. The total energy of the bremsstrahlung beam was monitored with a thick-walled ionization chamber throughout the experiment. The accuracy in measuring the total energy is estimated to be less than 3%.[16]

A liquid hydrogen target utiliging a small mechanical refrigerator was used in the experiment.[17] Fig. 4 shows a schematic view of the target. Hydrogen gas from the hydrogen gas reservoir which was placed out side of the experimental area was cooled down with liquid nitrogen and then liquified into the condencer chamber by a GB12-refrigerator. When the

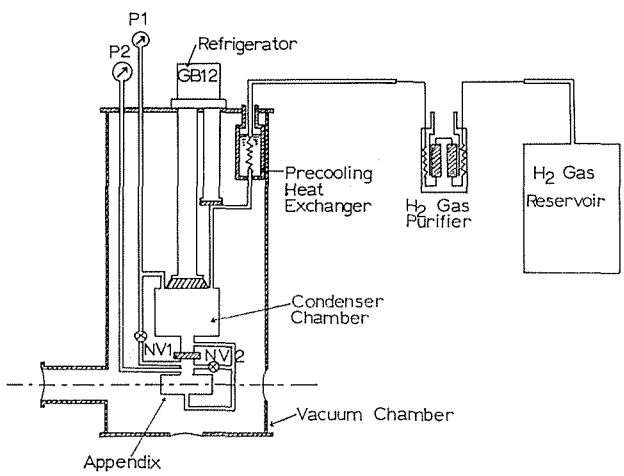

Fig. 4. Schematic diagram of the liquid hydrogen target system.

valves, NV–1 and NV–2, controled by pressurized helium gas were opened, liquid hydrogen in the condencer chamber flew into the liquid hydrogen container (appendix). When both valves were closed, the liquid hydrogen in the container went back to the condencer chamber. This procedure which fill the container with liquid hydrogen or evacuate liquid hydrogen from the container took us only about 3 minutes.

The liquid hydrogen container was a cylindrical shape of 60 mm in diameter and 120 mm in length, and was made of Mylar of 75 μm thick. The wall of the vacuum chamber was also made of Mylar of 175 μm thick. During the experiment, the pressure and temperature of liquid hydrogen in the container had been kept at one atmospheric pressure and 20.4° K, respectively.

2-3 π° meson detector

Two photons from a π° meson were detected with a pair of photon detectors which consisted of a lead glass Cerenkov counter of total absorption type, a scintillation counter hodoscope, a lead plate converter, a pair of scintillation counters, and a LiH hardener. A shematic view of one of the photon detectors is shown in Fig. 5. The informations on the energies of both photons and on the correlation angle between the two photons were obtained from the pulse heights of the Cerenkov counters and the addresses of the counter hodoscopes which were fired. These measurements made it possible to evaluate the energy and production angle of the π° meson with large precision by applying the method proposed by Tau.[18] The distribution of the correlation angles between the two photons from π° mesons having a constant energy has a sharp peak at the minimum correlation angle, ϕ_{min},

$$\cos \phi_{min}/2=P/E,$$

where P and E denote the momentum and the total energy of the π° meson, respectively. Therefore, in order to achieve the maximum detection efficiency for π° mesons, the angle between the photon detectors was chosen to be equal to the minimum correlation angle.

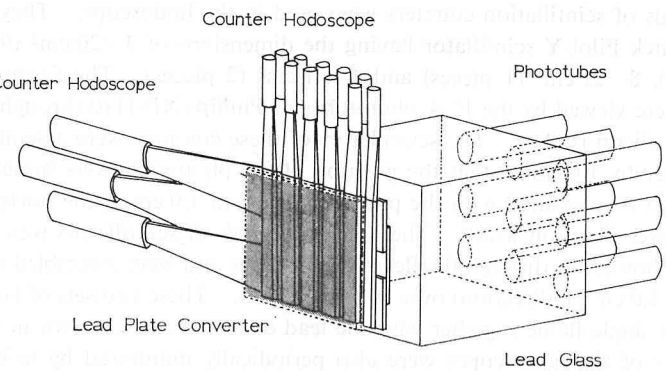

Fig. 5. Perspective view of the photon detector. LiH hardener is not described.

(a) Cerenkov counters[20]

The Cerenkov counter was made of a lead glass of 25 cm cube (8.8 radiation lengths) whose refractive index is 1.6477. The lead glass was painted with CM enamel and was viewed from one side with nine phototubes, RCA 6655A's, which were kept to contact optically close to the lead glass through silicon oil. Each phototubes was magnetically shielded with a μ-metal cylinder of 1 mm thick. The gains and timing of the nine phototubes were carefully adjusted by using attenuators and delay lines. The output signals from these phototubes were added together by an adder circuit.

The gains of the Cerenkov counters were calibrated with the monochromatic electron beam which was analyzed by the pair spectrometer shown in Fig. 1. At the calibration measurement the LiH hardeners were removed. In Fig. 6, the energy resolutions of the Cerenkov counter for three cases in which the thickness of the lead converter was 2, 1 and zero radiation lengths. The gain of the Cerenkov counters was periodically monitored by using a photodiode XP-21, which was placed on the front surface of the lead galss.

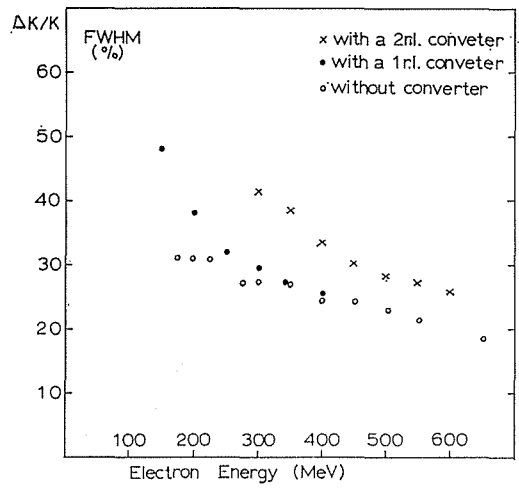

Fig. 6. Energy resolution of the Cerenkov counter. The measurements were made using monoenergetic electrons analysed with the pair spectrometer shown in Fig. 1. LiH hardener was taken off at the measurements.

(b) Scintillation counter hodoscope

Four kinds of scintillation counters were used in the hodoscope. They were made of the 6.4 mm thick Pilot-Y scintillator having the dimensions of 3×20 cm^2 (9 pieces), 2×20 cm^2 (2 pieces), 8×21 cm^2 (1 pieces) and 4×21 cm^2 (2 pieces). The former two kinds of scintillators were viewed by the $1''$ ϕ phototubes of Phillips XP-1110 through a flexible light pipe made of silicon rubber. The scintillators of these counters were assembled to overlap with each other by 1.0 cm so that the position of the photon showers initiated in the lead converter could be measured with the precision of about 1.0 cm in the horizontal direction (x-direction) over 21 cm in width. The other two kinds of scintillators were viewed by the RCA 6655A phototubes through the flexible light pipes and were assembled to overlap with each other by 4.0 cm (Y-direction) over 20 cm in width. These two sets of hodoscopes were mounted on a single flame together with the lead converter, as is shown in Fig. 5. Gains of all counters of the hodoscopes were also periodically monitored by using the electron beam of several hundred MeV and by measuring the single counts during the experiment.

(c) Veto counters and LiH hardeners

A pair of veto counters were placed in front of the hodoscopes to reject charged particles. Each counter consisted of the scintillator having the dimension of 120 mm+250 mm$\times$6.4 mm which was viewed by a phototube RCA 6655A through a light guide made of lucite. In front of these veto counters, a LiH hardener of 0.2 radiation lengths was placed to absorb low energy photons. This hardener also reduced low energy charged particle backgrounds. Gains of veto counters were continuously monitored by measuring the single counts at about every thirty minutes.

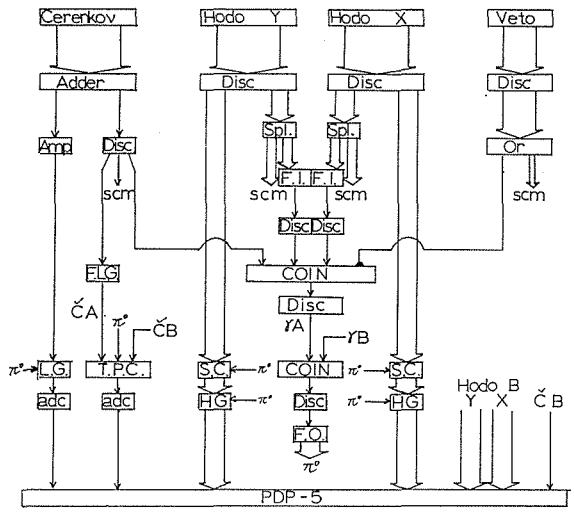

Fig. 7. Block diagram of the electronics. All accidental channels and monitor channels are omitted in this diagram except for the single count monitor channels. The notations are: Disc, discriminator; Amp, amplifier; Spl, splitter; Or, or-circuit; F. I., fan-in; Coin, coincidence; FLG, fast linear gate; LG, slow linear gate; SC, strobed coincidence; HG, Hodoscope gate; FO, fan out; adc, analog-to-digetal convetor; scm, single count monitor.

2-4 Electronics

A block diagram of the electronic system is shown in Fig. 7. Signals from the Cerenkov counter, any one of the hodoscope X, any one of the hodoscope Y and from the veto-counter of each photon detector were fed into a logic circuit through the discriminator circuits, so that the coincidence signals ($\bar{V}\cdot HX\cdot HY\cdot C$) called the γ-signals were produced. The coincidence signal between the two γ-signals from the both photon detectors, which was called the π°-signal, was used as a gate pulse to open many circuits such as the linear gates and the ADC (ND 160F) for both Cerenkov counters, the strobed coincidence circuits for all the hodoscopes, the time-to-pulse height converter (TPC) and the PDP–5 data processor. The gating time for the linear gate, the strobed coincidence circuit and the TPC were 50 ns, 20 ns and 100 ns respectively. When the π°-signals was produced the PDP–5 data processor was interupted and brought into the program mode state to record the flowing informations into its core memories: (1) Pulse heights of both Cerenkov counters, (2) The time differences between two photons, and (3) the address of the hodoscope counters which were fired by the photon showers initiated in the lead converters. During the measurement, at the rest of time the PDP–5 data processor displayed the two dimensional spectrum of two photon energies or the spectrum of the time difference on a CRT. After about five hundred events were stored, these data were transfered on a paper tape with a teletype (ASR–35). The tape thus obtained were processed by PDP–5, PDP–7 and OKITAC 4300 data processors with off-line mode.

In addition to the electronic system described above, logic circuits produced the coincidence signals (V.HX.HY.C) for both photon detectors. This signals were called the charged signals and monitored with the INS 10Mc scalers during the experimant.

2-5 Calibration of the Detection Efficiency of the π° Detector

The detection efficiencies of the γ°-meson detector were measured by detecting both recoiled proton and π° meson produced in the reaction $\gamma p \rightarrow \pi^\circ p$ with the experimental arrangement shown in Fig. 3. The recoiled protons were detected with a magnetic spectrometer and clearly separated from positive pions by measuring flight time between S_1 and S_3 counters and also by inserting a Cu absorber between S_3 and S_4 counters. The coincidence signal of these scintillation counters (S_1,S_2,S_3,$\bar{S}_4$) served as the master pulse of the proton detection system and the gate pulse of the TPC. The flight time spectrum was stored into a TMC 100 channel PHA.

The π° mesons were measured with the system described before with only one exception that one more information on the coincidence between proton signal and π° signal was added.

The detection efficiency was evaluated from the following ratio,

$$\eta = \frac{N(\pi^\circ p)}{N(p)}$$

where $N(\pi^\circ p)$ and $N(p)$ are the coincidence rate between the π° meson and recoiled proton and the counting rate of protons, respectively. The results are presented in Table 1, where the results of the Monte Carlo calculation are also listed. They agree well each other within the experimental and calculation errors.

Table 1. Detection efficiencies. The measured values of the detection efficiency for π° mesons of the three different momentum are presented. The calculated values by the Monte Carlo method are also listed for comparison.

Momentum of Tagged π° Meson (MeV)	$\theta_{\pi^\circ}^{\mathrm{Lab}}$ (deg.)	Coincidence Event Rate	Detection Efficiency	
			Experimental Value ($\times 10^{-3}$)	Monte Calro Simuration($\times 10^{-3}$)
870	29.1	199	6.21 ± 0.44	6.19 ± 0.35
535	32.5	137	2.39 ± 0.20	2.38 ± 0.18
364	34.6	10	0.78 ± 0.25	1.14 ± 0.17

During this calibration measurement, the differential cross sections at about 50° in the energy range between 500 and 1100 MeV were obtained simultaneously from the counting rate of π° mesons.

By varing the excitation current of the spectrometer, the effect of the background events from double π° mesons production was measured and it was evaluated to be negligibly small compared with the other errors of differential cross sections.

3. Data Reduction

The differential cross sections of the reaction $\gamma p \rightarrow \pi^\circ p$ were obtained with the following procedure;

(a) discrimination of the background events from the informations on the time difference, the total energy of two photons and the mass of π° mesons,
(b) corrections of the measured counting rate,
(c) Monte Carlo calculation of the detection efficiency, and
(d) reduction of the differential cross sections.

3-1 Rejection of Background Events

The time-to-pulse height convertor of Culligan & Lipman type produces no output signal when the start pulse is preceded by the stop pulse.[21] Therefore those events without

output pulse of TPC can be considered as accidental events. The amounts of these events for each measurements ranged from 6% to 36% of the total events for the zero degree measurements. A typical time difference is shown in Fig. 8.

The maximum energy of the bremsstrahlung beam was always set at about 150 MeV

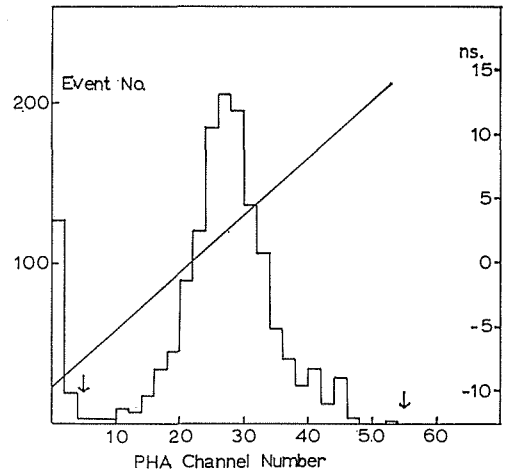

Fig. 8. Typical spectrum of the flight time difference between two photons from the π° meson. The accepted area is shown with arrows. Time scale is also presented.

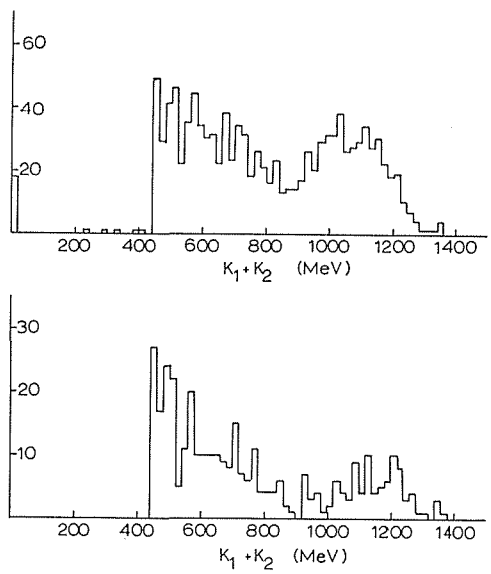

Fig. 9(a). Total energy spectrum of π° mesons which were detected with the full aperture of both photon detectors. The π° events are not clearly separated from the background events due to the broad energy acceptance of the detection system.

Fig. 9(b). Total energy spectrum of π° mesons which were detected with the inner half-side of both photon detectors. The π° events are well separated from the background events due to the narrowed energy acceptance of the detection system.

higher than the photon energy corresponding to the central momentum of the π° detection system. Fig. 9 shows the total energy spectrum of two photons. As is shown in Fig. 9(a), there are many background events from the electromagnetic process at the low energy side of the total energy spectrum of two photons from the π° meson. In Fig. 9(a), it seems that the separation of π° events from background events is not good because of a wide acceptance of our detection system. The total energy spectrum of two photons from π° mesons detected with a narrowed acceptance in which only inner sides of both photon detectors were permitted to be acceptable is shown in Fig. 9(b). It shows us that our detection system has a sufficient energy resolution to separate π° events from background events. It is also considered that there are some π° events from the double pion production process in the spectrum. These latter background events must have kinematically total energies at most 150 MeV smaller than the endpoint energy of the bremsstrahlung. Therefore those events which had total energies 250 MeV smaller than the endpoint energy were rejected to reduce these background events negligibly small.

The measured correlation angles between two photons told us the masses of mother particles through the following kinematical relation,

$$\mu=2k_1 \cdot k_2 (1-\cos\phi)$$

where μ, k_i, ϕ denote the mass of the mother particle, the photon energy and the correlation angle between the two photons, respectively. Therefore only those events between 50–200 MeV in the mass spectrum were accepted as π° meson events.

The amounts of the background events rejected by these criterions ranged from 2% to 35%. These criterions were requested in the Monte Carlo calculation as will be described in the following section.

3-2 Corrections of the measured counting rate

As was described previously, the photon detectors were set at very small angles for the most of the measurements, therefore all counters of the photon detectors were operated at fairly high counting rates. The electronic system used in this experiment can accept the counting rate up to 30 Mc. Therefore, the counting loss of the veto-counters amounted zero to 5% at most. However, the counting rate of the events that two charged particles were recorded as the γ-events in both photon detector was negligibly small, because the coincidence rate of two charged signals (V, HX, HY, C)$\times$2 was smaller than 20% of the π° coincidence rate at most. When the accidental coincidence occured between the veto counter and the other counters such as HX, HY and C in the one of the photon detectors, the true π° events were lost accidentally, because the events in which the two γ-signals ($\bar{\text{V}}$, HX, HY, C) coincided were recorded as the π° events. The counting loss due to this reason was evaluated to be 0.5–4% from the average counting rates of the veto counters and the time resolution of the veto coincidence which was 10 nsec. The uncertainty in evaluating this loss came mainly from the uncertainty of the time structure of the beam spill.

For the good events in which a single or adjacent counters in the hodoscope were fired, it was possible to evaluate the correlation angle between two photons. The energies and production angles of the π° mesons and the incident photon energies for the good events were evaluated event by event by applying the method proposed by Tau. However, due to the heavy backgrounds from low energy electrons and photons, there were some events in which two or three distinct counters were fired. These events are called as "HODO-out" events. The energy and the mass distributions discussed in Section 3–2 for the good events and the "HODO-out" events have the same distribution. Therefore the "HODO-out"

events were assumed to be the π°-events and added to the yields obtained from the good events by multiplying a correction factor.

3-3 Monte Carlo Simulation

The detection efficiency and the solid angle of the detection system for the π° mesons were fairly complicated. They were evaluated with the Monte Carlo simulation method, in which the experimental and data reduction procedures were repeated exactly. The results of the simulation were obtained as events rates versus the incident photon energy and the production angle of the π° mesons.

In the simulation, the followings were taken into account.

(a) The energy spectrum of the bremsstrahlung were approximated with the Schiff's formula integrated over all angles.

(b) The intensity distribution of photon beam across the beam line was assumed to have the Gaussian distribution with the standard deviation of 1.1 cm. The errors due to this assumption was estimated to be negligibly small. The finite lenngth of the target container was also taken into account. This was the main source of the energy resolution of the detection system for measurements at the extreme forward angle, because the correlation angle between two photons was evaluated with the approximation that the reaction point was considered to be the center of the target container.

(c) The cross section was assumed to be constant in the whole energy and angular regions. This assumption was confirmed to give no noticable error in evaluating the cross sections.

(d) The conversion efficiencies of photons in the LiH hardeners and in the lead converters were taken into account. The LiH hardeners were assumed to absorb 15.5% of incoming photons of 100—1000 MeV. The conversion efficiencies of the lead converters for photons into electron pairs were approximated in the following formula

$$\eta_{conv}=1-\exp(-\mu\cdot X)$$

$$\mu=0.0299\log_{10}K+0.0322$$

where X and K were the depth of the lead plate in radiation length and the energy of incoming photon in MeV, respectively. The energy loss of photons was also taken into account depending on the photon energies.

(e) The pulse height spectrum of the Cerenkov counters was assumed to have the Gaussian distribution with the relative pulse height resolution defined as follows;

$$\triangle k_i/k_i=D/\sqrt{k_i-\delta k_i},$$

where D and δk were a constant (4.85) and the energies lost in lead converters in MeV, respectively. The dependence of the pulse height on the incident position of the photon into the Cerenkov counter was also taken into account in the simulation. This dependence was also measured by the momentum analysed electron beam.

(f) The hodoscope used in this experiment was the scintillation counter hodoscope of overlapping type. Therefore, there were two kinds of channels. The first one required the firing of only one counter and the second one required the firing of two counters overapping each other. The incident positions of photons were measured by detecting the shower electrons with the hodoscopes. Therefore the channel width of the first kind seemed to be narrower than that of the second one because of the finite demension of the showers. This effect was shown in Fig. 10 and was taken into account in the simulation.

(g) Three dimensional momentum of the π° meson was reduced from the informations on the photon energies (k_1,k_2) and the correlation angle (ϕ) by using the following relations according to the procedure described in ref. 18 and 19,

$$k_1 \cdot k_2 = \mu^2 / [2(1-\cos\phi)],$$
$$k_1 + k_2 = E_{\pi^\circ},$$
$$\sin\theta_1 / \sin(\phi - \theta_1) = k_2/k_1,$$

where θ_1 was the angle between the flight directions of the photon denoted "1" and the π° meson.

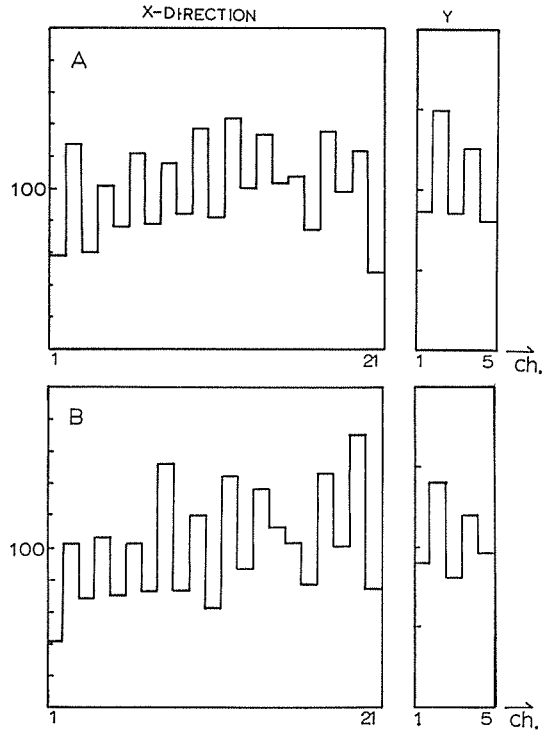

Fig. 10. Distribution of showers in the hodoscope. The yields of the odd channels are distinctly small. These channels correspond to those which require only one counter to be fired, while the even channels require two overlapping counters to be fired. The even channels work as wider channels than the odd ones because of the finite size of showers.

The energy and angular resolutions of the detection system were estimated event by event from the following value,

$$\triangle k = k' - k^\circ$$
$$\triangle\theta_{cm} = \theta'_{cm} - \theta^\circ_{cm}$$

where prime and small circle denoted the reconstructed values and the initial values in the simulation, respectively.

In the region far from the peak of the two dimentional spectrum (energy and angle) of simulated events, there were considered that the precision of the simulation was poor.

Therefore the data bins with small number of events (less than 30% of the peak value) were not used to evaluate the differential cross sections.

3-4 Reduction of the Differential Cross Sections

The experimental yield can be represented by the following formula,

$$Y=\int dk\int d(\cos\theta^*)\int d\phi^*\,\frac{d\sigma}{d\Omega^*}\,\eta\cdot\eta_{conv}\cdot N_T N(k)$$

with k : energy of incident photon,
θ^*,ϕ^*, : production angle of π° mesons in the CM system of the reaction $\gamma p\rightarrow\pi^\circ p$,
$d\sigma/d\Omega^*$: differential cross section,
η : detection efficiency for the π° meson,
η_{conv} : conversion efficiency of photons in the lead converter,
N_T : number of nucleons in the target
$N(k)$: number of incident photons.

On the other hand, the Monte Carlo simulation gives the following quantity,

$$Y_M=\int dk\int d(\cos\theta^*)\int d\phi^*\eta\cdot\eta_{conv}\cdot N_M(k)/2C_r$$

with $N_M(k)$: number of incident photons generated by random number in the simulation,
C_r : correction factor of the restricted regions of π° production angle and flight direction of decayed photons in the π° rest system. A factor two was multiplied because two photons are symmetric each other.

Finally the differential cross sections can be described as

$$\frac{d\sigma}{d\Omega^*}=Y/\int N(k)\,dk\int d(\cos\theta^*)\int d\phi^*\,\eta\cdot\eta_{conv}\cdot N_T$$

$$=\frac{Y}{Y_M}\,\frac{N_M(k)\,dk}{N(k)\,dk}\,\frac{1}{2C_rN_T}$$

$$=\frac{Y}{Y_M}\,\frac{J}{Q}\,\frac{1}{2C_rN_T}$$

with Q : equivalent quanta irradiated the hydrogen target in the experiment,
J : total repitition number of the simulation.

Using the experimental yield Y after corrected as discussed in Section 3–3, the differential cross sections were finally obtained as follows;

$$\frac{d\sigma}{d\Omega^*}=\frac{M}{Y_M}\left(\frac{F}{T}-\frac{E}{t}\right),$$

with $M=\dfrac{J}{Q}\,\dfrac{1}{2C_r.N_T}$ for unit count of beam integrator,

F,E : total yields in the same data bin of the full target and empty target runs, respectively,
T,t : counts of beam integrator of the full target and empty target runs, respectvely.

4. Experimental Results

4-1 Differential Cross Sections

The differential cross sections at angles smaller than 7° obtained with the arrangement shown in Fig. 1 are listed in Table 2–1, and are shown in Fig. 11. The widths of data bins were chosen to be almost equal to the energy resolutions of the detection system. They are ±25 MeV at the two measurements of the highest energy (k_0=1200 and 1150 MeV), ±20 MeV at the next three measurements (k_0=1050, 1100 and 950 MeV), and ±15 MeV at the rest measurements. The angular width of each data point is estimated to be ±1° (standard deviation) at higher energies and ±3° (standard deviation) at lower energies, while the angular resolution of the detection system is slightly better than those widths.

The angular dependences of the differential cross sections are summerized in Table 2–2 and shown in Fig. 12 (a)–(i). These data were obtained with two different experimental arrangements. The data at 20° and 30° of the lower energies and 15° and 20° of the higher energies were obtained with the arrangements shown in Fig. 2, and the other larger angles data were obtained with the arrangements shown in Fig. 3. The latter measurements gave larger errors in angles and energies compared with the former measurements.

The angles presented in Table 2–1 and 2–2 are the weighted mean values of all events in each data bins.

Table 2–1. Differential cross sections near zero degree. The presented errors include statistical errors, uncertainties of the "Hodo-out" events corrections, and count loss uncertainties of veto counters. Systematic errors common to all measurements are not included. (see text)

K_{max} (MeV)	k (MeV)	θ^{cm} (deg.)	$d\sigma/d\Omega$ (μb/str.)	$\triangle(d\sigma/d\Omega)$ (μb/str.)
500	350	6.1	6.96	0.82
550	400	6.0	6.67	0.64
600	420	4.4	5.01	0.69
	450	5.8	3.86	0.39
650	470	4.9	3.37	0.48
	500	5.6	3.51	0.34
700	520	4.3	2.34	0.31
	550	4.6	2.03	0.19
	580	5.9	1.70	0.16
750	570	4.2	1.84	0.29
	600	5.0	1.51	0.14
	630	5.5	1.19	0.12
	660	7.0	1.14	0.12
800	620	4.8	1.68	0.22
	650	4.6	1.29	0.12
	680	4.6	0.843	0.094
	710	4.4	0.683	0.081
	740	3.4	0.692	0.115
850	670	4.6	0.868	0.155
	700	5.3	0.640	0.082
	730	5.3	0.808	0.100
	760	5.8	0.707	0.087
	790	7.0	0.633	0.108

950	760	3.9	0.526	0.085
	800	4.4	0.560	0.060
	840	4.9	0.497	0.049
	880	5.0	0.454	0.049
	920	5.0	0.393	0.067
1000	810	4.3	0.584	0.091
	850	4.5	0.407	0.066
	890	5.1	0.349	0.045
	930	4.6	0.176	0.052
1050	860	3.7	0.385	0.073
	900	4.1	0.318	0.046
	940	5.1	0.187	0.042
	980	5.6	0.219	0.043
	1020	6.3	0.346	0.058
1150	950	2.8	0.321	0.090
	1000	4.4	0.141	0.061
	1050	4.4	0.292	0.046
	1100	4.0	0.271	0.051
1200	975	3.8	0.381	0.062
	1025	4.3	0.293	0.038
	1075	4.8	0.249	0.036
	1125	5.1	0.276	0.030
	1175	3.6	0.455	0.057

Table 2–1. Differential cross sections at large angles. The presented errors are the same as those in Table 2–1.

K (MeV)	k (MeV)	θ^{cm} (deg.)	$d\sigma/d\Omega$ (μb/str.)	$\Delta(d\sigma/d\Omega)$ (μb/str.)
700	520	17.7	3.46	0.84
		31.5	2.57	0.32
	550	18.4	2.34	0.48
		32.2	2.42	0.22
		47.9	2.57	0.27
	580	18.8	2.27	0.29
		32.9	1.95	0.19
		48.4	1.99	0.24
	610	19.2	1.73	0.32
		33.5	1.56	0.15
		50.6	1.66	0.21
	640	20.1	1.36	0.24
		33.7	1.74	0.20
		53.8	1.63	0.26
1150	950	13.2	1.72	0.25
		19.8	2.13	0.25
		33.4	2.99	0.46
		47.6	2.19	0.30
	1000	13.5	1.40	0.16
		20.2	1.63	0.14
		35.0	2.42	0.23
		47.4	2.04	0.21
	1050	13.8	1.01	0.12
		20.7	1.73	0.12
		36.2	2.34	0.19

	47.8	2.61	0.21
1100	15.6	0.670	0.108
	21.1	1.64	0.13
	34.5	2.10	0.24
	48.4	2.51	0.22

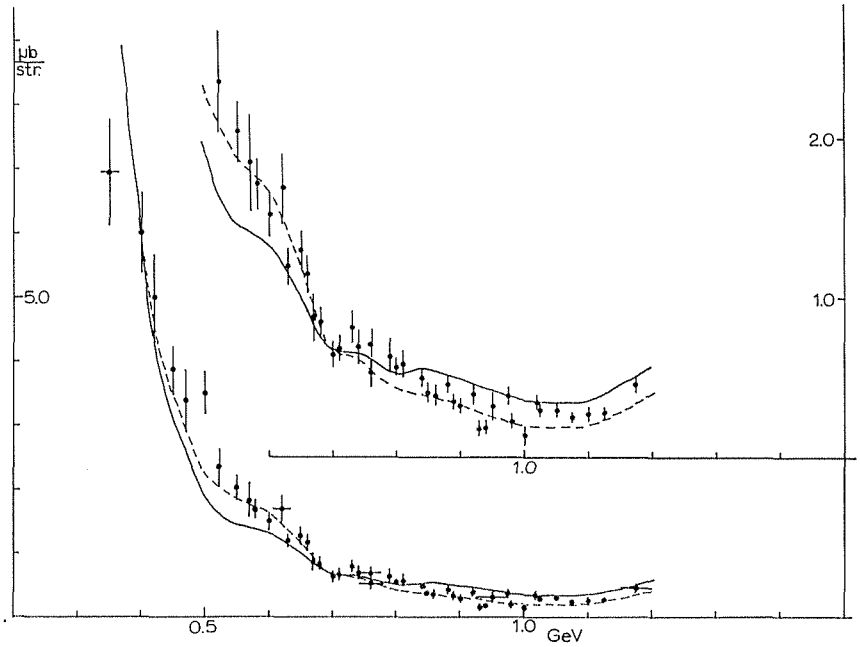

Fig. 11. Energy dependence of the differential cross sections of the reaction $\gamma P \to \pi^\circ P$ near zero degree. The data presented here are those at the angles smaller than 7 degrees. The energy width of the data points are shown in some typical cases. The solid curve shows the prediction of Walker's original amplitudes. The dashed curve shows the value of our modified amplitudes. (see text)

Fig. 12. (a)—(i) (following pages. 177—179)

Angular dependences of the differential cross sections at the incident photon energies of (a) 520 MeV, (b) 550 MeV, (c) 580 MeV, (d) 610 MeV, (e) 640 MeV, (f) 960 MeV, (g) 1000 MeV, (h) 1050 MeV and (i) 1100 MeV. Large angle data of other groups are also shown. ⏀ represents K. Berkelman, et al., ϕ ; V. L. Highland, et al., ⏃ ; C. Bacci, et al., ⏄ ; G. Belletlini, et al., ⏅ ; R. Diebold, et al., ⏆ ; C. Ward, et al., ⏇ ; R. M. Talman, et al., ⏈ ; G. Sauvage, et al. and ⏉ ; ours. The solid curves are the prediction of original Walker amplitudes (see text). The curves in Fig. 12(d) and (e) are the values at 600 MeV and 650 MeV, respectively.

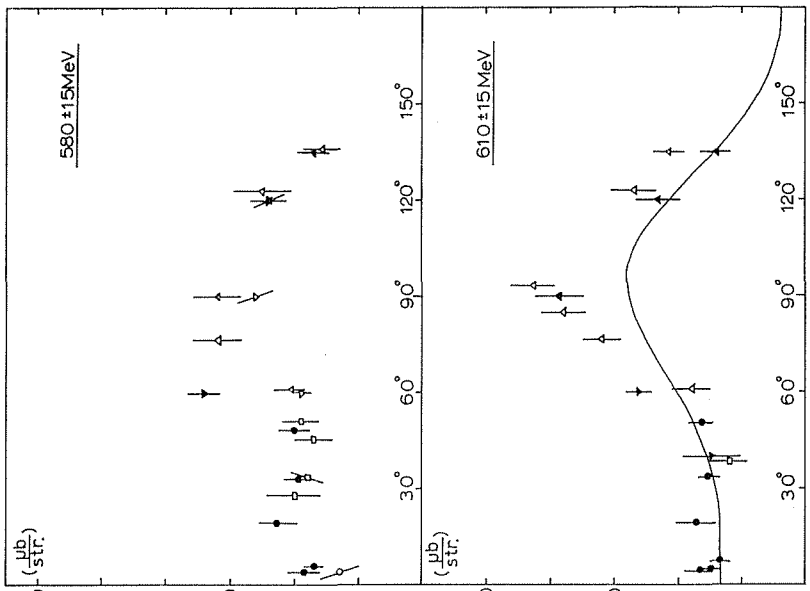

Fig. 12. (c), (d)

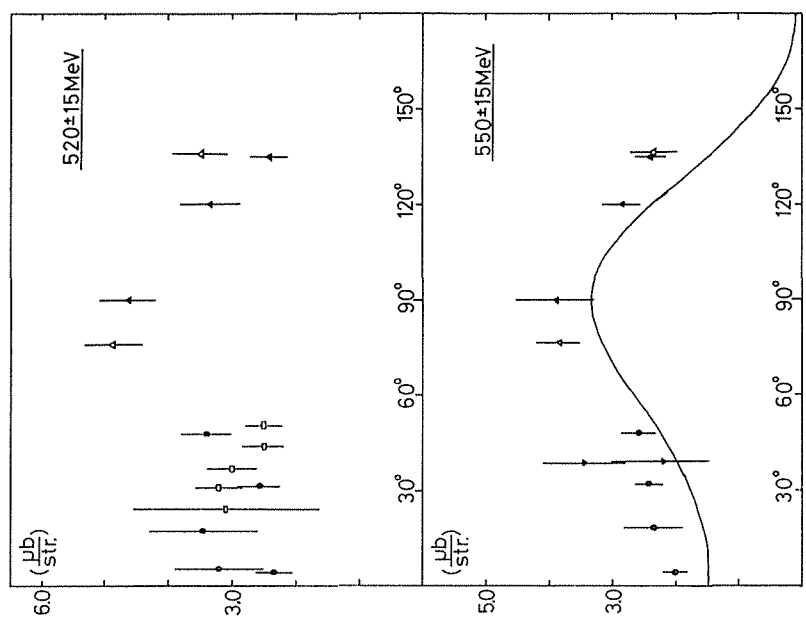

Fig. 12. (a), (b)

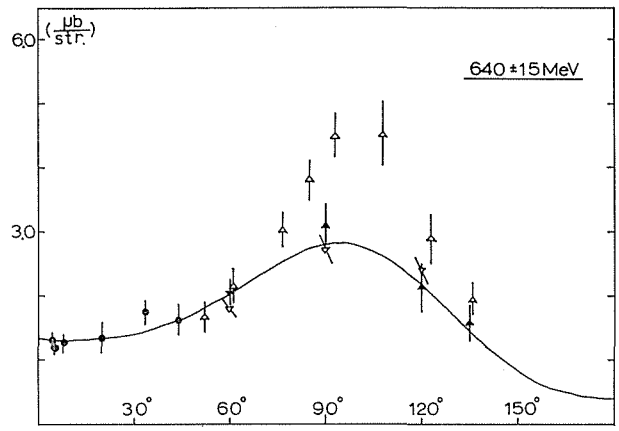

Fig. 12. (e)

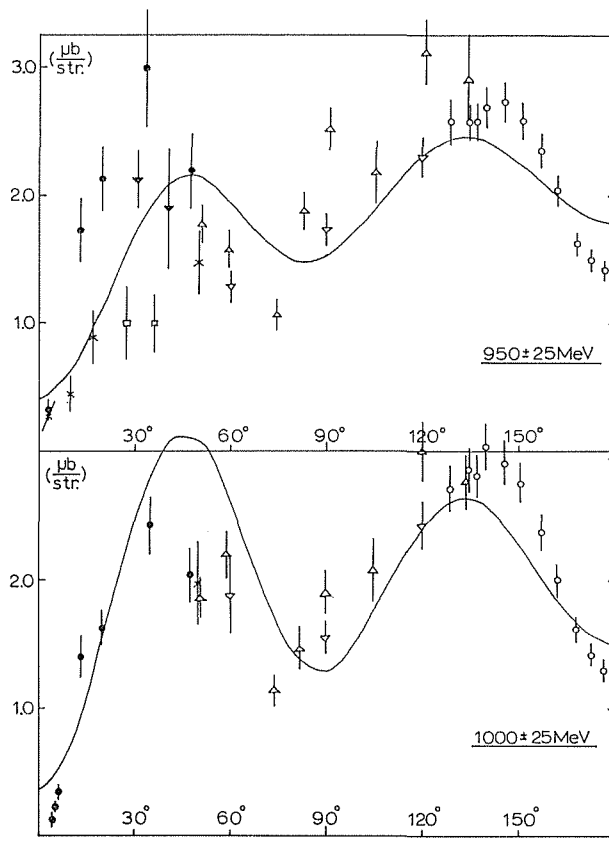

Fig. 12. (f), (g)

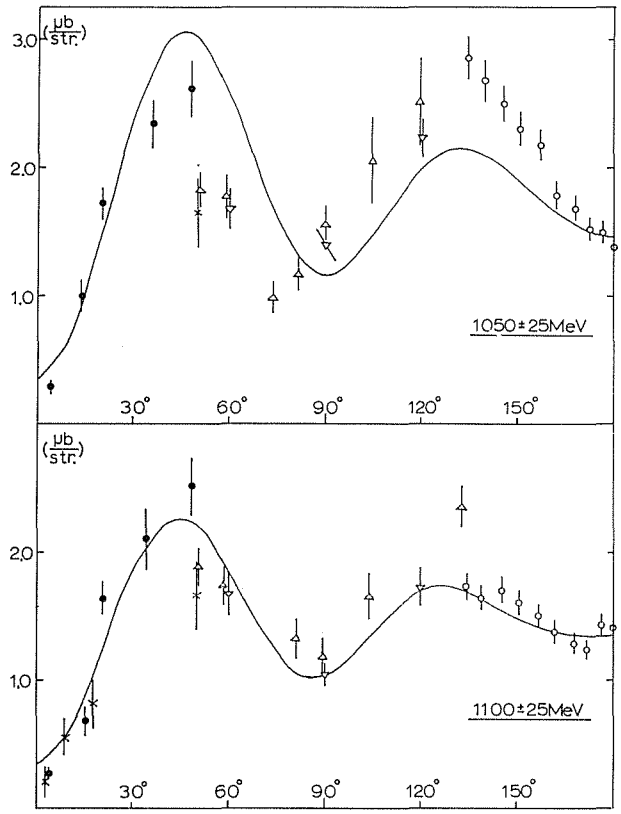

Fig. 12. (h), (i)

4-2 Errors

The errors presented in Table 2–1, 2–2, Fig. 11 and 12(a)–(i) include only the following errors,

(i) statistical errors of the experiments and of the Monte Carlo simulations (6—12%),
(ii) errors of the corrections due to the "HODO-out" events (1—3%),
(iii) errors of the corrections due to the counting loss of veto counters arising from the very high counting rate (0.2—1%).

These errors depend on individual measurement, and the first ones are the largest errors for all measurements. Other systematic errors common for all measurements are;

(i)	uncertainty of the total flux of the bremsstrahlung beam	3%
(ii)	uncertainty of the end point energy	2%
(iii)	uncertainty of the effective apperture of the photon detectors	3%
(iv)	uncertainty of the conversion efficiency	4%
(v)	uncertainty of the nucleon number in the target container	1%

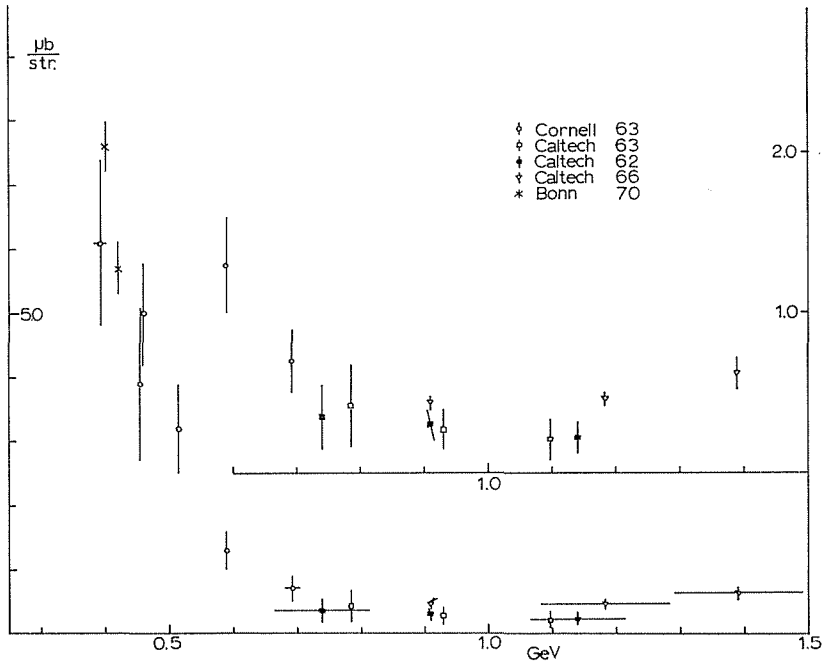

Fig. 13. Energy dependence of the differential cross sections of the reaction $\gamma p \to \pi^0 p$ near zero degree measured at other laboratories. The energy width of the data points are also presented.

The quadrature sum of these errors is about 6%. This systematic errors should be taken into account to the errors presented in Table 2–1 and 2–2.

5. Discussion

Fig. 13 shows the energy dependence of the differential cross sections of the reaction $\gamma p \to \pi^0 p$ near zero degree ($\lesssim 7°$) which were measured by other groups.[22)-25)] Comparing Fig. 11 and Fig. 13, they seem to have a very similar feature in gross structure and to be in a fairly good agreement in absolute values.

In Fig. 12(a)–(i) there are also shown the large angle data measured at other laboratories. In the energy range from 520 MeV to 640 MeV (Fig. 12(a)–(e)), one can see a general feature that there is no angular dependence up to about 60° in the CM system. The agreement between our data and those of other groups is fairly good. On the other hand, the energy is higher, the peaks around 90° become higher. But the flat dependences at forward angle do not change. It may be difficult to reproduce theoretically the sharp peaks around 90° and the plateau below 60° simultaneously. It seems to be very important to measure a systematic measurement of the angular dependence at these energies in the wide angular range.

Fig. 12(f)–(i) shows angular dependence in the energy range from 950 MeV to 1100 MeV. Our data agrees well with those of Caltech at extreme forward angles, but, generally speaking, are higher than other data at other angles.

The differential cross sections of the π^0 photoproduction at 180° were measured by several groups.[33)-37)] Most of them exhibit small but sufficiently noticeable peaks at the second and the third resonance energies. But our data do not show such an evidence at 0°.

The DESY's data say that only $I=3/2$ resonances are dominantly excited at 180°.[36] It seems that only P_{33} (1236) and F_{37} (1920) resonances are excited also at 0° (see Fig. 11 and Fig. 13).

Fujii, et al., [38]showed the evidence of η-cusp effect in the differential cross sections of the reaction $\gamma p\to\pi^+ n$ at 180°. There is seen the similar effect at the energy of 700 MeV in Fig. 11, though it is not so definit.

Table 3. Best fit values of the partial wave analysis. The original values of Walker's analysis and the prediction of a quark model are also presented.

Amplitude	Best fit values $(\mu b)^{1/2}$	Original Walker's amplitudes $(\mu b)^{1/2}$	Quark Model Prediction $(\mu b)^{1/2}$
$A_{0+}[S_{11}(1561)]$	0.266	0.460	1.3
$A_{1-}[P_{11}(1471)]$	0.493	0.177	0.14
$A_{1+}[P_{33}(1236)]$	not modified	1.414	1.2
$A_{2-}[D_{13}(1519)]$	0.866×10^{-1}	0.140	0.11
$A_{2+}[D_{15}(1652)]$	-0.312×10^{-2}	not included	0.0
$A_{3-}[F_{15}(1672)]$	-0.667×10^{-2}	not included	$<10^{-3}$

Recently Walker had made a partial wave analysis of the single pion photoproduction using almost all of the available data including those of neutron target reaction.[14] His amplitudes farly well describe the data over whole energy range below 1.3 GeV. But, as shown in Fig. 11, there are some discrepancies between our data and the prediction of Walker's amplitudes around 500 MeV. For a quantitative discussion we modified his amplitudes to reproduce our data more sufficiently by following his scheme of analysis. Although his analysis contains many parameters, we modified only resonance amplituds. The best fit values are listed in Table 3 where the Walker's original values are also presented for comparison. Our result requires a rather large P_{11} excitation in the pion photoproduction from protons. It contradicts with the prediction of simple quark model by Copley, et al.[4] A similar result was recently obtained by Devenish, et al. in the partial wave analysis using a resonante saturated dispersion relation.[39]

ACKNOWLEDGEMENTS

The auther would like to express his sincere thanks to Prof. S. Yasumi, Prof. K. Miyake and Prof. T. Nakamura for their continuous encouragements and guidances through this work. He is deeply grateful to Dr. H. Itoh, Dr. S. Kobayashi, Dr. Y. Hemmi, Mr. H. Yoshida, Mr. N. Tamura, Mr. T. Inagaki, Mr. Y. Inagaki and Mr. N. Yamashita for their advices and collaboration in carring out this experiment.

Thanks are also due to the members of the synchrotron operation crew of Institute for Nuclear Study for their nice operation, and due to the members of the target group for their preparing effort of the new target. His thanks are also due to Mr. J. Tsukamoto, Mr. S. Ohya, Mr. M. Yoshioka and Mr. A. Ando for their support for preparing counters and so on.

REFERENCES

1) H. J. Lipkin: Phys. Lett. **12** (1964) 154.
2) R. G. Moorhouse: Phys. Rev. Lett. **16** (1966) 772.
3) A. Donnachie: Phys. Lett. **24B** (1967) 420.

4) L. A. Copley, G. Karl and E. Obryk: Phys. Lett. **29B** (1969) 117, Nucl. Phys. **B13** (1969) 303.
5) D. S. Beder: Nuovo Cimento **33** (1964) 94.
6) S. D. Eckland and R. L. Walker: Phys. Rev. **159** (1967) 1195.
7) W. Schmidt: Z. Phys. **182** (1964) 76.
G. Höhler and W. Schmidt: Ann. Phys. **28** (1964) 34.
8) D. Schwela, H. Rollnik, R. Weizel and W. Korth: Z. Phys. 202 (1967) 452.
D. Schwela and R. Weizel: Z. Phys. **221** (1969) 71.
9) F. A. Berends, A. Donnachie and D. L. Weaver: Nucl. Phys. **B4** (1967) 1, 54, 103.
10) Recently two energy independent analyses are done in the first resonance region.
P. Noelle and W. Pfeil: Nucl. Phys. **B31** (1971) 1.
F. A. Berends and D. L. Weaver: Nucl. Phys. **B30** (1971) 575.
11) T. Yamaki: Prog. Theor. Phys. **38** (1967) 153.
12) Y. C. Chau, N. Dombey and R. G. Moorhouse: Phys. Rev. **163** (1967) 1632.
13) R. G. Moorhouse and W. A. Rankin: Nucl. Phys. **B23** (1970) 181.
14) R. L. Walker: Phys. Rev. **182** (1969) 1729.
15) T. Fujii, A. Imanishi, M. Kasuya and T. Yamakawa: Japanese Journal of Applied Physics **10** (1971) 774.
16) A. Kusumegi, T. Miyachi, K. Narushima, I. Sato and S. Watanabe: Japanese Journal of Applied Physics **10** (1971) 766.
17) Y. Doi, T. Fujii, T. Kitami, H. Okuno and K. Takamatsu: Japanese Journal of Applied Physics **10** (1971) 468.
18) L. Tau: Nucl. Instr. Methods **34** (1965) 352.
19) Y. Hemmi: Memoirs of the Faculty of Science, Kyoto Univ., Series A of Physics, Astrophysics, Geophysics and Chemistry **33** (1971) 339.
20) Y. Hemmi, R. Kikuchi, S. Kobayashi, K. Miyake, T. Nakamura, H. Okuno, S. Yasumi and Y. Yoshimura: Nucl. Instr. Methods **56** (1967) 213.
21) G. Culligan and N. H. Lipman: Rev. Sci. Instr. **31** (1960) 1209.
22) V. L. Highland and J. W. Dewire: Phys. Rev. **132** (1963) 1293.
23) R. M. Talman: Ph. D. Thesis, Caltech, 1963: R. M. Talman, C. R. Clinesmith, R. Gomez and A. V. Tollstrup: Phys. Rev. Lett. **9** (1962) 177.
24) G. L. Hatch: Ph. D. Thesis, Caltech, 1966.
25) E. Hilger, H. J. Roegler, L. M. Simons and M. Tonutti: Bonn Univ., PI 1–103, Juli 1970.
26) P. Spillantini and V. Valente: CERN-HERA 70–1, June 1970.
27) K. Berkelman and J. A. Waggoner: Phys. Rev. **117** (1960) 1364.
28) C. Bacci, G. Penso, G. Salvini, C. Mencuccini, A. Reale, V. Silvestrini, M. Spinetti and B. Stella: Phys. Rev. **159** (1967) 1124.
29) G. Bellettini, C. Bemporad, P. J. Biggs, P. L. Braccini, T. Del Prete and L. Foa: Nuovo Cimento **44** (1966) 239.
30) R. Diebold: Phys. Rev. **130** (1963) 2089.
31) C. Ward, B. Kenton and C. York: Phys. Rev. **159** (1967) 1176.
32) G. Sauvage: Thesis, LAL 1207, Orsay 1969.
33) H. De Staebler, E. F. Erickson, A. C. Hearn and C. Schaerf: Phys. Rev. **140** (1965) B336.
34) G. L. Cassiday, H. Fisher, A. Ito, C. Loh and J. Rutherfoord: Phys. Rev. Lett. **21** (1968) 933.
35) B. Delcourt, J. Lefrancois, G. Parrour, J. P. Perez-Y-Jorba and G. Sauvage: Phys. Lett. **29B** (1969) 70.
36) G. Buschhorn, P. Heide, U. Kotz, R. A. Lewis, P. Schmuser and H. J. Skronn: Phys. Rev. Lett. **20** (1968) 230.
37) M. Croissiaux, E. B. Dally, R. Morand, J. P. Pahin and W. Schmidt: Phys. Rev. **164** (1967) 1623.
38) T. Fujii, H. Okuno, S. Orito, H. Sasaki, T. Nozaki, F. Takasaki, K. Takikawa, K. Amako, I. Endo, K. Yoshida, M. Higuchi, M. Sato and Y. Sumi: Phys. Rev. Lett. **26** (1971) 1672.
39) R. C. E. Devenish, D. H. Lyth and W. A. Rankin: Phys. Lett. **36B** (1971) 394.